AIAA JOURNAL
Vol. 31, No. 4, April 1993

# Finite Element Analysis of Large-Amplitude Panel Flutter of Thin Laminates

Iain R. Dixon* and Chuh Mei†
*Old Dominion University, Norfolk, Virginia 23529*

**Large-amplitude panel flutter of thin rectangular composite laminates is studied using finite elements. The principle of virtual work is used to develop the equations of motion of a fluttering rectangular panel. The large deflections are represented by von Karman strain-displacement relations and the aerodynamic load is represented by the use of the quasisteady first-order piston theory. The equations of motion are solved by implementing the lineared updated-mode with a nonlinear time function (LUM/NTF) approximation. Critical flutter values and limit-cycle amplitudes for graphite-epoxy and boron-epoxy laminates at various boundary conditions, lamination orientations, and numbers of layers are investigated.**

## Nomenclature

| | |
|---|---|
| $a$ | = panel length |
| $[a_a]$, $[A_a]$ | = element/system aerodynamic influence matrices |
| $[A]$, $[B]$, $[D]$ | = extensional, coupling, and bending stiffness of a laminate |
| $c$ | = maximum deflection |
| $D_{11o}$ | = $D(1, 1)$ with all fibers aligned in the $x$ direction |
| $g_a$ | = nondimensional aerodynamic damping |
| $[g]$, $[G]$ | = element/system aerodynamic damping matrices |
| $[k]$, $[K]$ | = element/system linear stiffness matrices |
| $[m]$, $[M]$ | = element/system mass matrices |
| $[n1]$, $[N1]$ | = element/system first-order nonlinear stiffness matrices |
| $[n2]$, $[N2]$ | = element/system second-order nonlinear stiffness matrices |
| $u$, $v$, $w$, | = element displacement functions |
| $\{w\}$, $\{W\}$ | = element/system displacement vectors |
| $\alpha$ | = coefficient of thermal expansion |
| $\theta$ | = lamination angle |
| $\kappa$ | = eigenvalue |
| $\lambda$ | = nondimensional dynamic pressure |
| $\{\Phi\}$ | = mode shape |
| $\Omega$ | = complex panel motion parameter |
| $\omega_o$ | = reference frequency |

*Subscripts*

| | |
|---|---|
| $a$ | = aerodynamic |
| $b$ | = bending |
| $c$ | = coupling |
| $cr$ | = critical |
| $l$ | = linear, limit cycle |
| $m$ | = membrane |
| $nl$ | = nonlinear |
| $\theta$ | = slope |

Presented as Paper 91-1173 at the AIAA/ASME/ASCE/AHS/ASC 32nd Structures, Structural Dynamics, and Materials Conference, Baltimore, MD, April 8-10, 1991; received Jan. 10, 1992; revision received July 14, 1992; accepted for publication July 27, 1992. 

*Graduate Research Assistant, Department of Mechanical Engineering and Mechanics; presently Associate Engineer, Lockheed Engineering and Sciences Company, Hampton, VA 23666. Member AIAA.

†Professor, Department of Mechanical Engineering and Mechanics. Associate Fellow AIAA.

## Introduction

THE investigation into the effects of air flowing at supersonic speeds over aircraft structures has been conducted in detail. Pressure distributions from the airflow may influence the aircraft in several ways. One concern, panel flutter, occurs when the aerodynamic pressure becomes great enough to make the panel vibrate in a self-excited state. The panel is usually configured in such a way that one side of it is exposed to the airflow and the other side is part of a structural cavity, as shown in Fig. 1. The onset of flutter may cause a catastrophic failure; however, in many cases, due to the material and configuration of the plate, a fatigue failure is possible. It is probable that the flutter oscillations will have a large deflected amplitude; thus it is important to investigate the limit-cycle motions as well as the flutter boundaries.

Two survey articles which give an overview of panel flutter theories and tests are given by Dowell[1] and Reed et al.[2] Classical solutions of nonlinear isotropic panel flutter are found usually through the use of Galerkin's method in the spatial domain and found by techniques such as numerical integration,[3-5] perturbation,[6,7] and harmonic balance[7,8] in the time domain. An extension of the classical study into orthotropic plates was conducted by Eslami[9] and Librescu[10] using the harmonic balance method. Finite elements analysis of linear panel flutter was first reported by Olson[11,12] for two- and three-dimensional cases. Yang and Sung[13] studied three-dimensional isotropic panel flutter as well. An extension of the finite element method into nonlinear oscillations of two-dimensional isotropic panels was given by Mei,[14] Rao and Rao,[15] Sarma and Varadan,[16] and Gray et al.[17] In addition to flutter of two- and three-dimensional isotropic plates, Xue and Mei[18-20] also considered the effects of temperature. Mei and

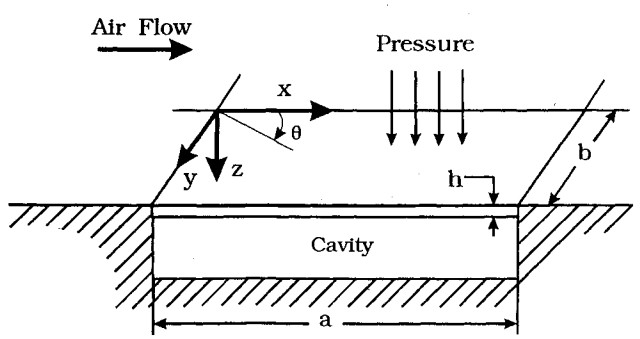


**Fig. 1 Schematic of an aircraft panel subjected to an aerodynamic load.**

Weidman[21] and Han and Yang[22] extended the finite element methods to nonlinear, three-dimensional rectangular and triangular isotropic plates. The study of nonlinear flutter of composite plates was investigated by Dixon and Mei[23,24] and Liaw and Yang.[25]

A finite element analysis of large-amplitude panel flutter of arbitrarily laminated composite plates is presented here. The element and system equations of motion are derived using the principle of virtual work. The solution procedure details the linearized updated mode with a nonlinear time function (LUM/NTF) approximation which determines the limit-cycle motions. Results which investigate the effects of varying the boundary conditions, lamination orientations, and numbers of layers of graphite-epoxy and boron-epoxy laminates follow.

## Mathematical Formulation

### Rectangular Finite Element

The following derives the system equations of motion for a composite plate in flutter. The plate considered has a length $a$, width $b$, and thickness $h$. The air flows along the $x$ axis and edges are either simply supported or clamped. Using rectangular elements with six degrees-of-freedom per node, the plate is discretized into a certain number of finite elements. The 24-element nodal displacements are separated into out-of-plane (bending) and in-plane (membrane) displacement components:

$$\{w\} = \begin{Bmatrix} w_b \\ w_m \end{Bmatrix} \tag{1}$$

The component $\{w_b\}$ is comprised of $w$, $w_x$, $w_y$, $w_{xy}$ and the component $\{w_m\}$ is comprised of $u$ and $v$. The element bending displacements $w$ are approximated with a bicubic function and the element membrane displacements, $u$ and $v$, are approximated with bilinear functions

$$\begin{aligned} w = {} & a_1 + a_2x + a_3y + a_4x^2 + a_5xy + a_6y^2 + a_7x^3 + a_8x^2y \\ & + a_9xy^2 + a_{10}y^3 + a_{11}x^3y + a_{11}x^3y + a_{12}x^2y^2 + a_{13}xy^3 \\ & + a_{14}x^3y^2 + a_{15}x^2y^3 + a_{16}x^3y^3 \end{aligned} \tag{2}$$

$$u = b_1 + b_2x + b_3y + b_4xy \tag{3}$$

$$v = b_5 + b_6x + b_7y + b_8xy \tag{4}$$

The time-dependent generalized coordinates, $\{a\}$ and $\{b\}$, are related to the nodal displacements by their respective transformation matrices given by

$$\{a\} = [T_b]\{w_b\} \tag{5}$$

and

$$\{b\} = [T_m]\{w_m\} \tag{6}$$

From the large deflection von Karman strain-displacement relations, the strain can be written as

$$\begin{Bmatrix} \epsilon_x \\ \epsilon_y \\ \gamma_{xy} \end{Bmatrix} = \begin{Bmatrix} \epsilon_x^o \\ \epsilon_y^o \\ \gamma_{xy}^o \end{Bmatrix} + z\begin{Bmatrix} \kappa_x \\ \kappa_y \\ \kappa_{xy} \end{Bmatrix} \tag{7}$$

where $\{\epsilon^o\}$ and $\{\kappa\}$ represent the in-plane and bending (curvature) strain vectors, respectively. The strains and curvatures in terms of the displacement functions are

$$\begin{Bmatrix} \epsilon_x^o \\ \epsilon_y^o \\ \gamma_{xy}^o \end{Bmatrix} = \begin{Bmatrix} u_{,x} \\ v_{,y} \\ u_{,y} + v_{,x} \end{Bmatrix} + \frac{1}{2}\begin{Bmatrix} w_{,x}^2 \\ w_{,y}^2 \\ 2w_{,x}w_{,y} \end{Bmatrix} \tag{8}$$

$$\begin{Bmatrix} \kappa_x \\ \kappa_y \\ \kappa_{xy} \end{Bmatrix} = -\begin{Bmatrix} w_{,xx} \\ w_{,yy} \\ 2w_{,xy} \end{Bmatrix} \tag{9}$$

Transverse shear strains are neglected because of the thin-plate assumption, thus $\gamma_{yz}$ and $\gamma_{xz}$ are not included. The in-plane strains in Eq. (8) can be represented as

$$\{\epsilon^o\} = \{\epsilon_m^o\} + \{\epsilon_\theta^o\} = \{\epsilon_m^o\} + \tfrac{1}{2}[\theta]\{G\} \tag{10}$$

where the strain vector due to the large deflections, $\{\epsilon_\theta^o\}$, is separated into a product of the bending displacement's slopes. The components of this product are

$$[\theta] = \begin{bmatrix} w_{,x} & 0 \\ 0 & w_{,y} \\ w_{,y} & w_{,x} \end{bmatrix} \tag{11}$$

$$\{G\} = \begin{Bmatrix} w_{,x} \\ w_{,y} \end{Bmatrix} \tag{12}$$

The von Karman strains are represented in terms of the generalized coordinates and time-independent, spatial components as

$$\begin{aligned} \{\epsilon\} &= \{\epsilon_m^o\} + \{\epsilon_\theta^o\} + z\{\kappa\} \\ &= [C_m]\{b\} + \tfrac{1}{2}[\theta][C_\theta]\{a\} + z[C_b]\{a\} \end{aligned} \tag{13}$$

The stress-strain relations for the $k$th layer of a laminate with a lamination angle $\theta$ between the principal and the body axes are

$$\begin{Bmatrix} \sigma_x \\ \sigma_y \\ \tau_{xy} \end{Bmatrix}_k = \begin{bmatrix} \bar{Q}_{11} & \bar{Q}_{11} & \bar{Q}_{16} \\ \bar{Q}_{12} & \bar{Q}_{22} & \bar{Q}_{26} \\ \bar{Q}_{16} & \bar{Q}_{26} & \bar{Q}_{66} \end{bmatrix}_k \begin{Bmatrix} \epsilon_x \\ \epsilon_y \\ \gamma_{xy} \end{Bmatrix} \tag{14}$$

The matrix $[\bar{Q}]$ is the transformed reduced stiffness matrix comprised of the engineering constants and the influence of the lamination angle $\theta$.

From Eqs. (7) and (14), the stresses for the $k$th layer is then

$$\{\sigma\}_k = [\bar{Q}]_k(\{\epsilon^o\} + z\{\kappa\}) \tag{15}$$

The resulting forces and moments of the plate are determined by substituting Eq. (15) into

$$(\{N\}, \{M\}) = \int_{-h/2}^{h/2} \{\sigma\}_k(1, z)\, dz \tag{16}$$

Equation (16) is integrated over the thickness to obtain the forces and moments of a general laminate, where

$$\begin{Bmatrix} N \\ M \end{Bmatrix} = \begin{bmatrix} A & B \\ B & D \end{bmatrix} \begin{Bmatrix} \epsilon^o \\ \kappa \end{Bmatrix} \tag{17}$$

The matrices $[A]$, $[B]$, and $[D]$ are the extensional, coupling, and bending stiffnesses of the laminate, respectively.

The force and moment terms can be expanded in terms of the generalized coordinates [see Eq. (13)] where the force vector is comprised of membrane, slope, and bending terms:

$$\begin{aligned} \{N\} &= [A](\{\epsilon_m^o\} + \{\epsilon_\theta^o\}) + [B]\{\kappa\} \\ &= [A][C_m]\{b\} + \tfrac{1}{2}[A][\theta][C_\theta]\{a\} + [B][C_b]\{a\} \\ &= \{N_m\} + \{N_\theta\} + \{N_b\} \end{aligned} \tag{18}$$

The moment vector similarly becomes

$$\{M\} = [B](\{\epsilon_m^o\} + \{\epsilon_\theta^o\}) + [D]\{\kappa\}$$
$$= [B][C_m]\{b\} + \tfrac{1}{2}[B][\theta][C_\theta]\{a\} + [D][C_b]\{a\}$$
$$= \{M_m\} + \{M_\theta\} + \{M_b\} \tag{19}$$

**Equations of Motion**

The principal of virtual work is used to derive the equations of motion, where

$$\delta W = \delta W_{\text{int}} - \delta W_{\text{ext}} = 0 \tag{20}$$

The virtual work due to internal stresses, considered first, is

$$\delta W_{\text{int}} = \int_V \sigma_{ij}\delta\epsilon_{ij}\, dV \tag{21}$$

Taking the variation of the strain in Eq. (7) and substituting yields

$$\delta W_{\text{int}} = \int_A \left[ \int_{-h/2}^{h/2} \left(\{\delta\epsilon^o\}^t + z\{\delta\kappa\}^t\right)\{\sigma\}_k\, dz \right] dA \tag{22}$$

Thus, from Eq. (16), the internal virtual work becomes

$$\delta W_{\text{int}} = \int_A \left[\{\delta\epsilon^o\}^t\{N\} + \{\delta\kappa\}^t\{M\}\right] dA \tag{23}$$

The variation of the in-plane strains and curvatures become

$$\{\delta\epsilon^o\}^t = \{\delta b\}^t[C_m]^t + \{\delta a\}^t[C_\theta]^t[\theta]^t \tag{24}$$

and

$$\{\delta\kappa\}^t = \{\delta a\}^t[C_b]^t \tag{25}$$

After substituting Eqs. (18), (19), (24), and (25) into the internal virtual work equation, the following expression results:

$$\delta W_{\text{int}} = \int_A \Big[\left(\{\delta_b\}^t[C_m]^t + \{\delta a\}^t[C_\theta]^t[\theta]^t\right)\left([A][C_m]\{b\}\right.$$
$$\left. + \tfrac{1}{2}[A][\theta][C_\theta]\{a\} + [B][C_b]\{a\}\right) + \{\delta a\}^t[C_b]^t\left([B][C_m]\{b\}\right.$$
$$\left. + \tfrac{1}{2}[B][\theta][C_\theta]\{a\} + [D][C_b]\{a\}\right)\Big]\, dA \tag{26}$$

After transforming from generalized coordinates to nodal displacements using Eqs. (5) and (6), simplifying through, and separating into element stiffness matrices, the virtual internal work becomes

$$\delta W_{\text{int}} = \{\delta w_m\}^t\left([k_{mb}] + \tfrac{1}{2}[n1_{mb}]\right)\{w_b\} + \{\delta w_m\}^t[k_m]\{w_m\}$$
$$+ \{\delta w_b\}^t\left([k_b] + \tfrac{1}{2}[n1_b]_c + \tfrac{1}{2}[n1_b] + \tfrac{1}{3}[n2_b]\right)\{w_b\}$$
$$+ \{\delta w_b\}^t\left([k_{bm}] + \tfrac{1}{2}[n1_{bm}]\right)\{w_m\} \tag{27}$$

Refer to Ref. 24 for a more detailed derivation of the virtual work and element matrices. The element matrices $[k_b]$ and $[k_m]$ are linear bending and membrane stiffnesses, respectively. The linear element matrices $[k_{bm}]$ and $[k_{mb}]$ are due to the membrane-bending coupling laminate stiffness $[B]$. The first-order nonlinear stiffness matrices $[n1_{bm}]$, $[n1_{mb}]$, and $[n1_b]$ are linearly dependent on the deflections. Matrix $[n1_b]_c$ is from the large deflections and the coupling laminate stiffness. The second-order nonlinear stiffness $[n2_b]$ is quadratically dependent on the deflections.

The virtual work due to external forces is

$$\delta W_{\text{ext}} = \int_V B_i\delta u_i\, dV + \int_S T_i\delta u_i\, dS \tag{28}$$

In this case the body forces, which are defined by the inertia terms in each coordinate direction, is integrated through the thickness $h$. This is combined with the surface tractions, defined by an aerodynamic pressure term, to become

$$\delta W_{\text{ext}} = \int_A [\delta w(P_a - \rho h w_{,tt}) - \delta u(\rho h u_{,tt}) - \delta v(\rho h v_{,tt})]\, dA \tag{29}$$

The aerodynamic load $P_a$ is described by the first-order piston theory. This theory calculates the aerodynamic load on the panel from local pressures generated by the body's motion relative to the normal component of the air velocity.[1,3,26] The aerodynamic pressure, described in terms of slope and velocity components, is represented as

$$P_a = -\frac{2q}{\sqrt{M_\infty^2 - 1}}\left(w_{,x} + \frac{(M_\infty^2 - 2)}{(M_\infty^2 - 1)}\frac{1}{V}w_{,t}\right) \tag{30}$$

or

$$P_a = -\left(\lambda\frac{D_{11o}}{a^3}w_{,x} + \frac{g_a D_{11o}}{\omega_o a^4}w_{,t}\right) \tag{31}$$

where $q = \rho_a V^2/2$ is the dynamic pressure, $V$ is the airflow speed, $\rho_a$ is the air density, $M_\infty$ is the Mach number, and $a$ is the panel length. The constant $D_{11o}$ is the resulting $D(1, 1)$ value in the bending stiffness matrix for a unidirectional 0-deg laminate. The 0-deg angle is parallel to the $x$ axis and is the direction of the airflow. The nondimensional dynamic pressure and aerodynamic damping coefficient are given by

$$\lambda = \frac{2qa^3}{D_{11o}\sqrt{M_\infty^2 - 1}} \tag{32}$$

$$g_a = \frac{\rho_a V(M_\infty^2 - 2)}{\rho h\omega_o(M_\infty^2 - 1)^{3/2}} \tag{33}$$

where $\omega_o = (D_{11o}/\rho h a^4)^{1/2}$ is a reference frequency used to normalize the equations of motion. Equation (31) is substituted into the aerodynamic pressure term of the external virtual work equation. This constitutes the aerodynamic influence and damping matrices. The inertia terms in Eq. (29) are represented as mass matrices. The external work expressed in terms of the element mass, aerodynamic damping, and influence matrices becomes

$$\delta W_{\text{ext}} = \{\delta w_b\}^t\left(-\lambda[a_a]\{w_b\} - \frac{g_a}{\omega_o}[g]\{\dot w_b\}\right)$$
$$- \frac{1}{\omega_o^2}\{\delta w_b\}^t[m_b]\{\ddot w_b\} - \frac{1}{\omega_o^2}\{\delta w_m\}^t[m_m]\{\ddot w_m\} \tag{34}$$

Equations (27) and (34) are substituted into Eq. (20) to obtain the elemental equations of motion

$$\frac{1}{\omega_o^2}\begin{bmatrix} m_b & 0 \\ 0 & m_m \end{bmatrix}\begin{Bmatrix} \ddot w_b \\ \ddot w_m \end{Bmatrix} + \frac{g_a}{\omega_o}\begin{bmatrix} g & 0 \\ 0 & 0 \end{bmatrix}\begin{Bmatrix} \dot w_b \\ \dot w_m \end{Bmatrix}$$
$$+ \left(\lambda\begin{bmatrix} a_a & 0 \\ 0 & 0 \end{bmatrix} + \begin{bmatrix} k_b & k_{bm} \\ k_{mb} & k_m \end{bmatrix} + \frac{1}{3}\begin{bmatrix} n2_b & 0 \\ 0 & 0 \end{bmatrix}\right.$$
$$\left. + \frac{1}{2}\begin{bmatrix} (n1_b)_c + n1_b & n1_{bm} \\ n1_{mb} & 0 \end{bmatrix}\right)\begin{Bmatrix} w_b \\ w_m \end{Bmatrix} = \begin{Bmatrix} 0 \\ 0 \end{Bmatrix} \tag{35}$$

Equation (35) represents a nonstandard eigenvalue problem due to the skew symmetric orientation of the aerodynamic influence matrix $[a_a]$. The system equations of a composite plate in flutter, which are assembled from the elemental equations, are represented as

$$\frac{1}{\omega_o^2}[M]\{\ddot{W}\} + \frac{g_a}{\omega_o}[G]\{\dot{W}\} + \left(\lambda[A_a] + [K] + \frac{1}{2}[N1] + \frac{1}{3}[N2]\right)\{W\} = \{0\} \tag{36}$$

where, from Eq. (1)

$$\{W\} = \begin{Bmatrix} W_b \\ W_m \end{Bmatrix} \tag{37}$$

## Solution Procedure

Neglecting the in-plane inertia effects in Eq. (36) results in a relationship between the membrane displacements and the bending displacements described by

$$\{W_m\} = -[K_m]^{-1}\left([K_{mb}] + \tfrac{1}{2}[N1_{mb}]\right)\{W_b\} \tag{38}$$

Replacing $\{W_m\}$ in the system equations with Eq. (38) yields

$$\frac{1}{\omega_o^2}[M_b]\{\ddot{W}_b\} + \frac{g_a}{\omega_o}[G]\{\dot{W}_b\} + ([K]_l + [K]_{nl})\{W_b\} = \{0\} \tag{39}$$

where in this case, the linear stiffness matrix is

$$[K]_l = \lambda[A_a] + [K_b] - [K_{bm}][K_m]^{-1}[K_{mb}]$$

and the nonlinear stiffness matrix is

$$[K]_{nl} = -\tfrac{1}{2}[K_{bm}][K_m]^{-1}[N1_{mb}] + \tfrac{1}{2}[N1_b] + \tfrac{1}{2}[N1_b]_c + \tfrac{1}{3}[N2_b] - \tfrac{1}{2}[N1_{bm}][K_m]^{-1}\left([K_{mb}] + \tfrac{1}{2}[N1_{mb}]\right)$$

The solution of Eq. (39) is determined by assuming the deflection to be in the form of a single eigenvector, where

$$\{W_b\} = \bar{c}\{\Phi_b\}e^{\Omega t} \tag{40}$$

The vector $\{\Phi_b\}$ is generally complex and $\bar{c}$ is a nonzero scalar constant which represents the amplitude of the panel deflection. In the exponential term, $\Omega = \alpha + i\omega$ is the complex panel motion parameter. The variable $\alpha$ is the damping rate and $\omega$ is the frequency. Substituting the assumed response into Eq. (39) results in the following eigenvalue problem:

$$\bar{c}(-\kappa[M_b] + [K]_l + [K]_{nl})\{\Phi_b\}e^{\Omega t} = \{0\} \tag{41}$$

where the nondimensional eigenvalue is

$$\kappa = -(\Omega/\omega_o)^2 - g_a(\Omega/\omega_o)$$

The eigenvalue includes the damping coefficient so that the aerodynamic damping matrix can be absorbed in the mass matrix. This is possible since $[M_b] = [G]$.

By expressing $e^{\Omega t}$ as a complex quantity in Euler form and requiring both coefficients of sin $\omega t$ and cos $\omega t$ to vanish, then Eq. (41) can be written as two separate equations

$$\bar{c}e^{\alpha t}(-\kappa[M_b] + [K]_l + [K]_{nl})\{\Phi_b\}\cos\omega t = \{0\} \tag{42a}$$

$$i\bar{c}e^{\alpha t}(-\kappa[M_b] + [K]_l + [K]_{nl})\{\Phi_b\}\sin\omega t = \{0\} \tag{42b}$$

Since $\bar{c}$ is nonzero, Eq. (39) is for a constrained system and the solution is a nontrivial one. Equations (42a) and (42b) represent the same eigenvalue problem. To solve Eq. (42), the nonlinear matrix $[K]_{nl}$ needs to be evaluated. Also, since all of the system quantities used in developing Eq. (39) are real, it must be concluded that the nodal response quantities must also be as real. As is generally the case with most nonlinear problems, numerous methodologies are available to obtain linearized solutions.[13-25] Here, this is accomplished by employing the linearized updated-mode with a nonlinear time function (LUM/NTF) approximation.[17-20,23,24] Where, in the iterative solution procedure, the nonlinear stiffness $[K]_{nl}$ is reevaluated after each iteration using the updated panel deflection and the nonlinear time functions are approximated to simple harmonic functions by neglecting the higher harmonics. To evaluate element nonlinear stiffness matrices $[n1_{bm}]$, $[n1_{mb}]$, $[n1_b]_c$, and $[n2_b]$, the corresponding element displacement vectors $\{w_b\}$ are needed. They can be approximated from Eq. (40) by normalizing the eigenvector as follows. Recognizing that $\{w_b\}$ is real, take only the real part of the normalized Eq. (40)

$$\{W_b\} = \frac{\bar{c}e^{\alpha t}}{|(\Phi_b)_k|}\{|\Phi_b|\cos(\beta - \beta_k)\}\cos\omega t \tag{43}$$

The quantity $|(\Phi_b)_k|$ is the magnitude of the largest displacement component of the eigenvector $\{\Phi_b\}$ and $\beta_k$ is the corresponding phase angle. Next, denote $c = \bar{c}e^{\alpha t}$ as the damped amplitude. Thus, it is clear from Eq. (43) that the sign of the damping parameter controls the stability of the solution. The solution is stable for all $\alpha$ that are less than zero. When $\alpha$ is equal to zero, $c = \bar{c}$ and the resulting solution corresponds to that of a limit-cycle oscillation. By letting the normalized bending eigenvector be

$$\{\bar{\Phi}_b\} = \frac{1}{|(\Phi_b)_k|}\{|\Phi_b|\cos(\beta - \beta_k)\} \tag{44}$$

Eq. (43) becomes

$$\{W_b\} = c\{\bar{\Phi}_b\}\cos\omega t \tag{45}$$

Equation (45) results after Eq. (40) is normalized and scaled to a given limit-cycle amplitude $c$. Equation (45) is then used to approximate the various element displacements of the complete panel, $\{w_b\}$, and to evaluate the nonlinear element stiffness matrices. Reassembling to a system level, the nonlinear stiffnesses become a function of the displacement amplitude, its respective linearized stiffness, and a harmonic term, where

$$[N1_{mb}] = c[\overline{N1}_{mb}]\cos\omega t \tag{46}$$

$$[N1_{bm}] = c[\overline{N1}_{bm}]\cos\omega t \tag{47}$$

$$[N1_b]_c = c[\overline{N1}_b]_c\cos\omega t \tag{48}$$

$$[N2_b] = c^2[\overline{N2}_b]\cos^2\omega t \tag{49}$$

The nonlinear stiffness $[\overline{n1}_b]$ depends on the in-plane deflections, which are unknown up to this point. The system in-plane displacements can be obtained from Eqs. (38) and (45) to be

$$\{W_m\} = -[K_m]^{-1}\left([K_{mb}] + \tfrac{1}{2}[N1_{m\bar{b}}]\right)c\{\bar{\Phi}_b\}\cos\omega t \tag{50}$$

the assembled nonlinear stiffness matrix $[N1_b]$ becomes

$$[N1_b] = c[\overline{N1}_b]_1\cos\omega t + c^2[\overline{N1}_b]_2\cos^2\omega t \tag{51}$$

From collecting the nonlinear stiffnesses, the assembled global eigenvalue equation becomes

$$\kappa[M_b]\{\Phi_b\} \approx ([K]_l + [\bar{K}]_{nl})\{\Phi_b\} \tag{52}$$

where the linear stiffness matrix $[K]_l$ is shown in Eq. (39) and the linearized stiffness matrix becomes

$$[\bar{K}]_{nl} = -\frac{\sqrt{2}c}{4}[K_{bm}][K_m]^{-1}[\overline{N1}_{mb}] - [\overline{N1}_{bm}][K_m]^{-1}\left(\frac{\sqrt{2}c}{4}[K_{mb}] + \frac{3c^2}{16}[\overline{N1}_{mb}]\right) + \frac{\sqrt{2}c}{4}[\overline{N1}_b]_1 + \frac{3c^2}{8}[\overline{N1}_b]_2 + \frac{\sqrt{2}c}{4}[\overline{N1}_b]_c + \frac{c^2}{4}[\overline{N2}_b] \quad (53)$$

Refer to Ref. 24 for a more detailed discussion of the evaluation of linearized stiffness matrices.

To initiate the procedure, the linear vibration mode is first considered. From the eigenvalue equation the first mode shape is used to approximate the nonlinear stiffness matrices. Note

**Table 1 Composite material properties**

| | Graphite-epoxy | Boron-epoxy |
|---|---|---|
| $E_1$ | 30.0 | 30.0 Mpsi |
| $E_2$ | 0.75 | 3.0 Mpsi |
| $G_{12}$ | 0.375 | 1.0 Mpsi |
| $\nu_{12}$ | 0.25 | 0.30 |
| $\rho$ | $2.58799 \times 10^{-4}$ | $1.87629 \times 10^{-4}$ lb-s$^2$/in.$^4$ |

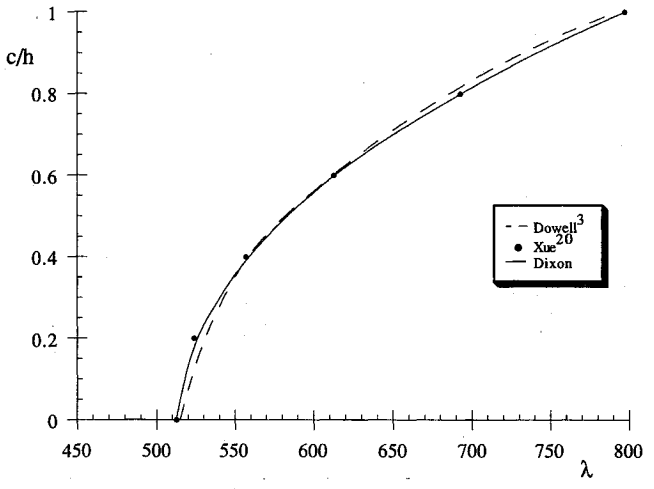


**Fig. 2 Comparison of nonlinear flutter of a simply supported isotropic panel.**

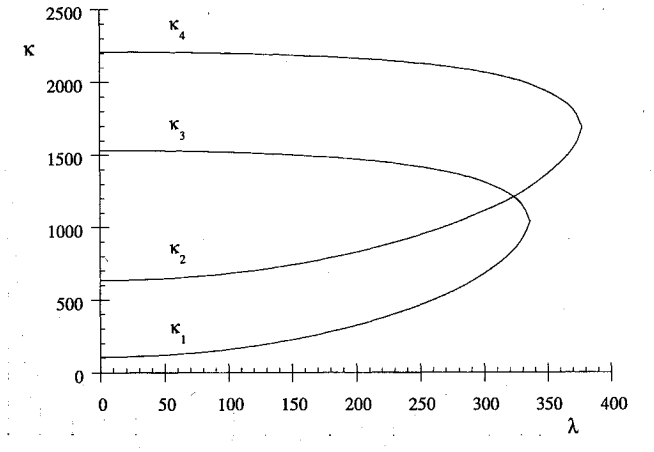


**Fig. 3 Coalescence of first four eigenvalues of a simply supported, three-layer, square cross-ply, graphite-epoxy laminate.**

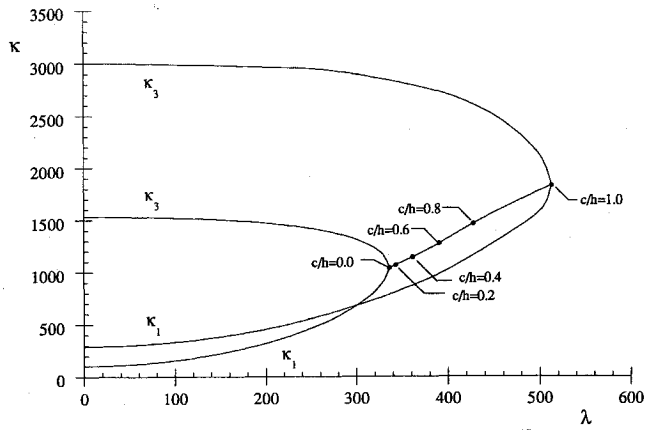


**Fig. 4 Coalescence of eigenvalues for nonlinear flutter of a simply supported, three-layer, square cross-ply, graphite-epoxy laminate.**

are then used to determine the linearized stiffness matrix $[\overline{N1}_b]$. The linearized stiffnesses are subsequently assembled, as shown in Eq. (53), and then used in the linearized eigenvalue problem. To see if the problem is completed, the convergence of the eigenvalue is checked. Normally if the error in the eigenvalues, after each iteration, is less than $10^{-6}$, convergence is considered to be achieved. If convergence was not achieved, the lowest eigenvector (mode shape) is used to update the linearized stiffness matrices, thus the problem is reiterated until a converged solution is obtained.

## Results

Two finite element grid sizes were used in the analyses. Orthotropic and isotropic panels are modeled as $3 \times 8$ "half plates," where eight elements lie along the direction of the air flow. This takes advantage of the symmetry of the panel flutter deflection. Anisotropic plates are modeled as $6 \times 8$ "full plates" since the shape of the flutter deflection may not be symmetric. Immovable in-plane boundary conditions are considered in all cases ($u = v = 0$ along edges). The dimensions considered for the "full plate" analyses are $12.0 \times 12.0 \times 0.12$ in. The composites considered are either graphite-epoxy or boron-epoxy where the material properties, from Jones,[27] are listed in Table 1.

To verify the solution of the nonlinear panel flutter analysis, comparisons are made between large-amplitude flutter of isotropic plates. Figure 2 shows a comparison between the present with Dowell[3] and Xue[20] for a limit-cycle amplitude vs dynamic pressure of a simply supported isotropic panel. In the first case, Dowell uses Runge-Kutta time numerical integration to obtain classical limit-cycle results using six free vibration modes. Xue uses a finite element formulation which utilizes the LUM/NTF solution approximation. Note that the damping parameter is 0.01 in Dowell's case while it is zero for the other two cases.

In the case of isotropic panels without the effects of aerodynamic damping $g_a$, the critical value at which flutter occurs is normally the point at which the first two eigenvalues, $\kappa_1$ and $\kappa_2$, coalesce. Intersection occurs just as they become complex conjugate pairs. If damping is taken into account, flutter would occur when the damping rate becomes positive and thus the panel motions become unstable.[14,21] This would increase the dynamic pressure required to instigate flutter as well as the limit-cycle motions. The effects of damping ($g_a = 0$) are neglected in the examples that follow, in which case more conservative results are obtained.

Unusual results have been found for selected composite laminates. Figure 3 shows the coalescence of the first four eigenvalues of a simply supported, square, three-layer cross-ply laminate. Note that for this particular case, the eigenvalues of the first two modes do not intersect. Coalescence occurs with the eigenvalues of the first and the third modes and with

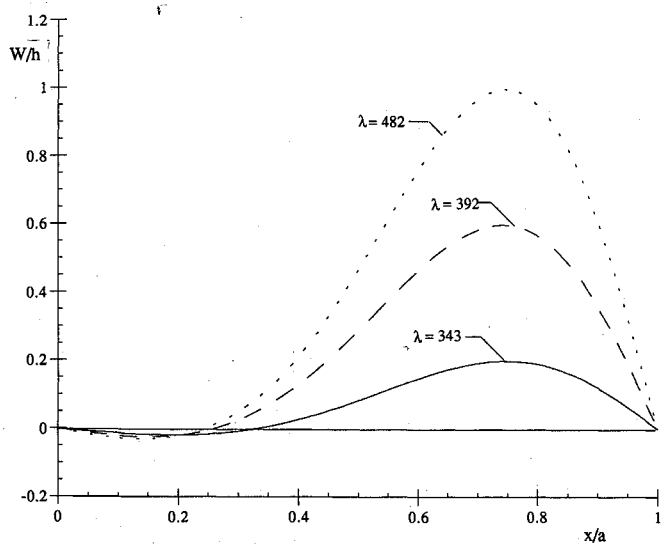


**Fig. 5 Limit-cycle deflection of a simply supported, square three-layer, cross-ply, graphite-epoxy panel.**

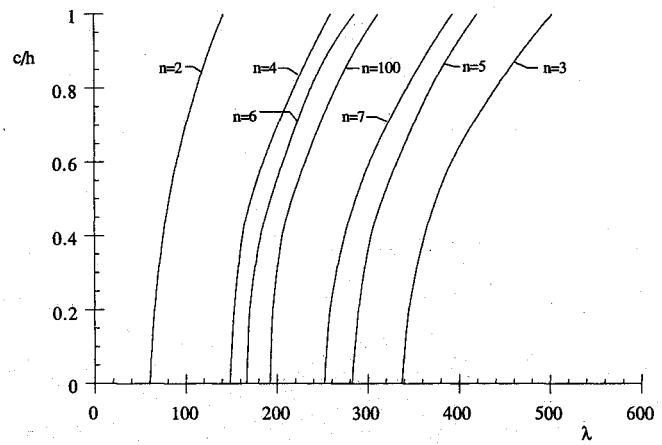


**Fig. 6 Limit-cycle amplitude vs dynamic pressure of simply supported, square symmetric and antisymmetric, cross-ply, graphite-epoxy laminates with various numbers of layers.**

the eigenvalues of the second and the fourth modes. The reason for the coalescence of the higher modes are due to the differences between $E_1$ and $E_2$. Graphite-epoxy, which has a high value of 40 for $E_1/E_2$, is used in this case. When the ratio of $E_1$ and $E_2$ is smaller, the coalescence characteristics more closely resemble isotropic panels.

The curves in Fig. 3 are from small-amplitude flutter and show the critical value of λ. The limit-cycle values are shown in Fig. 4, for the same laminate, along with the linear values. Coalescence of the first and third eigenvalues for the nonlinear cases (not shown for $c/h = 0.2, 0.4, 0.6, 0.8$) occurs in a similar fashion as the linear case.

Figure 5 shows the centerline deflection of a three-layer, graphite-epoxy cross-ply laminate. The deflection which is plotted is shown when $\lambda_l = 342.92$, $\lambda_l = 391.50$, and $\lambda_l = 481.56$. The nondimensional dynamic pressures correspond to limit-cycle amplitudes of 0.2, 0.6, and 1.0, respectively. A panel with no aerodynamic load would have a small-amplitude, sinusoidal mode shape as a free vibration. However, as the dynamic pressure increases beyond the critical value, the maximum deflection shifts in the direction of the airflow. This maximum occurs at a location three-quarters of the total panel length.

Limit-cycle motions of symmetric and antisymmetric laminates with variable numbers of layers, $n$, are examined. This case considers cross-ply laminations of graphite-epoxy with a constant total thickness of 0.12 in. Figure 6 shows limit-cycle amplitude vs dynamic pressure for the simply supported symmetric and antisymmetric cross-ply laminates with several numbers of layers. Symmetric composites are the laminates with an odd number of layers. A 0-deg fiber orientation for the first layer is considered here. A three-layer laminate is (0/90/0). Their configuration is symmetric with respect to the midsurface, thus there is no coupling stiffness [$B$]. Antisymmetric composites are the laminates with an even number of layers. The large coupling effects between the composite layers are accounted for in the coupling stiffness of these types of laminates. Interesting results have been discovered when studying these two types of composites. Note that there is a large difference in the critical dynamic pressure between a three-layer and a two-layer laminate (both of thickness 0.12 in.). Even though there is only a difference of one layer, the coupling stiffness is zero for the three-layer symmetric laminate and is relatively high for the two-layer antisymmetric laminate. The coupling between the extensional forces and bending moments has a detrimental effect on the ability for an antisymmetric laminate to resist flutter. As the number of layers increases in an antisymmetric laminate, the effect of the coupling stiffness decreases. It is also interesting to point out that the symmetric and antisymmetric curves converge to each other as the number of layers increase.

The characteristics of a clamped and a simply supported panel are compared with two semisimply supported panels; one with a clamped leading edge and one with a clamped trailing edge. The panels evaluated are square, three-layer,

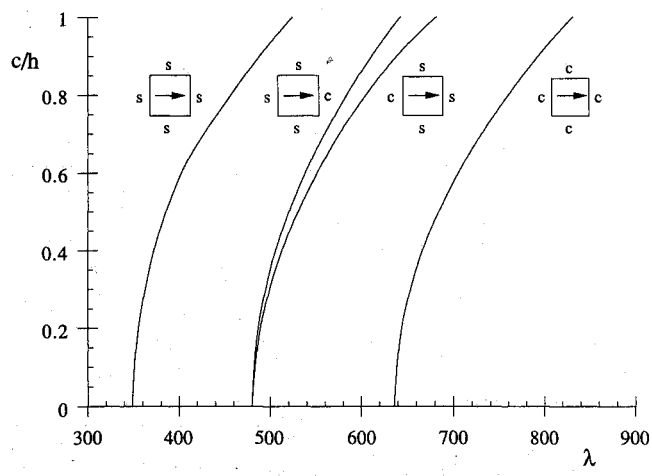


**Fig. 7 Effect of boundary conditions on a square three-layer, cross-ply, boron-epoxy laminate.**

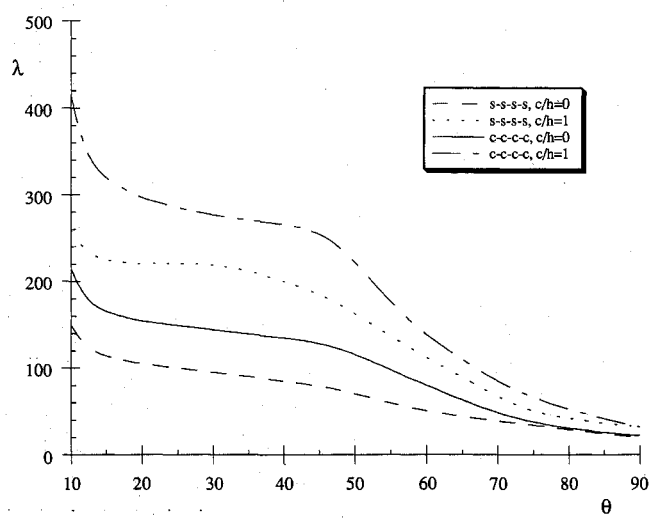


**Fig. 8 Limit-cycle and critical dynamic pressures of simply supported and clamped, three-layer, square angle-ply, graphite-epoxy laminates ($\theta/-\theta/\theta$).**

cross-ply laminates. The dynamic pressure is plotted in relation to the limit-cycle amplitude for a boron-epoxy plate in Fig. 7. As would be expected, the fully clamped and the simply supported panels bound the values of the panels that have multiple boundary conditions. An interesting point is that the panels with clamped leading and trailing edges have the same flutter critical point; however, the curves do differ in the nonlinear region. The slopes of the limit-cycle amplitude vs dynamic pressure curve for the simply supported panel are nearly identical to the panel with a clamped leading edge but the slopes of the clamped panel is sightly different than the panel with a clamped trailing edge. Figure 7 of Ref. 17 shows that the slopes of a clamped-clamped panel and a simply clamped panel have identical slopes for the two-dimensional case. Exact duplication of the slopes of these curves may not be possible in this case due to the boundary conditions of the edges parallel to the direction of the airflow. A nearly identical pattern would probably exist if these side edges of the fully clamped panel were simply supported.

The influence of the lamination angle $\theta$ on limit-cycle and critical dynamic pressures is investigated. Figure 8 relates the limit-cycle dynamic pressure, $\lambda_l$ $(c/h = 1.0)$, to its respective laminate orientation for three-layer, angle-ply $(\theta/-\theta/\theta)$ graphite-epoxy plates simply supported on all edges and clamped on all edges. For comparison, $\lambda_{cr}$ $(c/h = 0.0)$ is also plotted in Fig. 8 for various angles. The nonlinear and linear cases follow the same trend as $\theta$ changes. It is easily seen that a panel is most resistant to flutter when the fibers are nearly aligned to the direction of airflow. There are large differences in the values of between the four curves when there is a strong stacking sequence (low $\theta$). However, the differences become small for weak stacking sequences (high $\theta$). The interesting feature about this figure are the plateaus in the curves. The curves appear to level off between angles of 90–75 deg and between 45–15 deg. Conversely, relatively large increases occur between angles of 75–45 deg and 15 deg and less. A similar pattern was interestingly found in Ref. 28 for $\lambda_{cr}$ of angle-ply laminates.

## Conclusions

An analysis of nonlinear flutter of composite panels using a finite element method is presented. The corresponding governing equations of motion are formulated and the eigenvalue problem is solved by employing the principle of virtual work and the linearized updated mode with the nonlinear time function (LUM/NTF) approximation, respectively.

The formulation, which considers the first-order piston theory to model the aerodynamic pressure, provides a reasonable estimate of flutter, deflection shapes, and frequencies for thin plates at approximate Mach numbers of greater than $\sqrt{2}$. The problem yields a homogeneous set of equations which represents the "self-excited" oscillations caused by the aerodynamic load. This method has been verified by comparing classic six-mode results for nonlinear flutter of isotropic panels.

Results show that flutter and limit-cycle motions occur when the eigenvalues of the first and third modes coalesce. This is due to the differences in the engineering constants, $E_1$ and $E_2$. For a plate of constant thickness, a symmetric laminate is generally less likely to flutter than an antisymmetric laminate due to the coupling stiffness. The stiffness and limit-cycle characteristics of symmetric and antisymmetric laminates converge as the number of layers increase.

## References


[1]Dowell, E. H., "Panel Flutter: A Review of the Aeroelastic Stability of Plates and Shells," *AIAA Journal,* Vol. 8, No. 3, 1970, pp. 385–399.

[2]Reed, W. H., Hanson, P. W., and Alford, W. J., "Assessment of Flutter Model Testing Relating to the National Aero-Space Plane," NASP Contractor Rept. 1002, July 1987.

[3]Dowell, E. H., "Nonlinear Oscillations of a Fluttering Plate," *AIAA Journal,* Vol. 4, No. 7, 1966, pp. 1267–1275.

[4]Dowell, E. H., "Nonlinear Oscillations of a Fluttering Plate II," *AIAA Journal,* Vol. 5, No. 10, 1967, pp. 1856–1862.

[5]Ventres, C. S., and Dowell, E. H., "Comparison of Theory and Experiment for Nonlinear Flutter of Loaded Plates," *AIAA Journal,* Vol. 8, No. 11, 1970, pp. 2022–2030.

[6]Morino, L., "A Perturbation Method for Treating Nonlinear Panel Flutter Problems," *AIAA Journal,* Vol. 7, No. 3, 1969, pp. 405–411.

[7]Kuo, C. C., Morino, L., and Dugundji, J., "Perturbation and Harmonic Balance Methods for Nonlinear Panel Flutter," *AIAA Journal,* Vol. 10, No. 11, 1972, pp. 1479–1484.

[8]Eastep, F. E., and McIntosh, S. C., "Analysis of Nonlinear Panel Flutter and Response under Random Excitation of Nonlinear Aerodynamic Loading," *AIAA Journal,* Vol. 9, No. 3, 1971, pp. 411–418.

[9]Eslami, H., "Nonlinear Flutter and Forced Oscillations of Rectangular Symmetric Cross-Ply and Orthotropic Panels Using Harmonic Balance and Perturbation Method," Ph.D. Dissertation, Old Dominion Univ., Norfolk, VA, 1987.

[10]Librescu, L., "Aeroelastic Stability of Orthotropic Heterogeneous Thin Panels in the Vicinity of Flutter Critical Boundary," *Journal de Mechanique,* Vol. 4, 1965, pp. 51–76.

[11]Olson, M. D., "Finite Elements Applied to Panel Flutter," *AIAA Journal,* Vol. 5, No. 12, 1967, pp. 2267–2269.

[12]Olson, M. D., "Some Flutter Solutions Using Finite Elements," *AIAA Journal,* Vol. 8, No. 4, 1970, pp. 747–752.

[13]Yang, T. Y., and Sung, S. H., "Finite-Element Panel Flutter in Three-Dimensional Supersonic Unsteady Potential Flow," *AIAA Journal,* Vol. 15, No. 12, 1977, pp. 1677–1683.

[14]Mei, C., "A Finite-Element Approach for Nonlinear Panel Flutter," *AIAA Journal,* Vol. 15, No. 8, 1977, pp. 1107–1110.

[15]Rao, K. S., and Rao, G. V., "Large-Amplitude Supersonic Flutter of Panels with Ends Elastically Restrained Against Rotation," *Computers and Structures,* Vol. 11, March 1980, pp. 197–201.

[16]Sarma, B. S., and Varadan, T. K., "Nonlinear Panel Flutter by Finite-Element Method," *AIAA Journal,* Vol. 26, No. 5, 1988, pp. 566–574.

[17]Gray, C. E., Jr., Shore, C. P., and Mei, C., "A Finite Element Method for Large-Amplitude Two-Dimensional Panel Flutter at Hypersonic Speeds," *AIAA Journal,* Vol. 29, No. 2, 1991, pp. 290–298.

[18]Xue, D., Shore, C. P., and Mei, C., "Finite Element Two-Dimensional Panel Flutter at High Supersonic Speeds and Elevated Temperature," *Proceedings of the AIAA/ASME/ASCE/AHS/ASC 31st Structures, Structural Dynamics and Materials Conference* (Long Beach, CA), AIAA, Washington, DC, April 1990, pp. 1464–1475.

[19]Xue, D., and Mei, C., "Finite Element Nonlinear Flutter and Fatigue Life of 2-D Panels with Temperature Effects," *Proceedings of the AIAA/ASME/ASCE/AHS/ASC 32nd Structures, Structural Dynamics, and Materials Conference* (Baltimore, MD), AIAA, Washington, DC, April 1991, pp. 1981–1991.

[20]Xue, D., "Finite Element Frequency Domain Solution of Nonlinear Panel Flutter with Temperature Effects and Fatigue Life Analysis," Ph.D. Dissertation, Old Dominion Univ., Norfolk, VA, Aug. 1991; also *AIAA Journal,* Vol. 31, No. 1, 1993, pp. 154–162.

[21]Mei, C., and Weidman, D. J., "Nonlinear Panel Flutter—A Finite Element Approach," *Computational Methods for Fluid-Structure Interaction Problems,* ASME Winter Annual Meeting, edited by T. Belytschko, and T. L. Geers, American Society of Mechanical Engineers, New York, AMD-Vol. 26, Nov. 1977, pp. 139–165.

[22]Han, A. D., and Yang, T. Y., "Nonlinear Panel Flutter Using High-Order Triangular Finite Elements," *AIAA Journal,* Vol. 21, No. 10, 1983, pp. 1453–1461.

[23]Dixon, I., and Mei, C., "Finite Element Analysis of Nonlinear Flutter of Composite Panels," *Proceedings of the AIAA/ASME/ASCE/AHS/ASC 32nd Structures, Structural Dynamics and Materials Conference* (Baltimore, MD), AIAA, Washington, DC, April 1991, pp. 2002–2010.

[24]Dixon, I. R., "Finite Element Analysis of Nonlinear Panel Flutter of Rectangular Composite Plates Under a Uniform Thermal Load," M.S. Thesis, Old Dominion Univ., Norfolk, VA, Aug. 1991, pp. 18–28.

[25]Liaw, D. G., and Yang, T. Y., "Nonlinear Supersonic Flutter and Reliability of Uncertain Laminated Plates," *Proceedings of the AIAA/ASME/ASCE/AHS/ASC 32nd Structures, Structural Dynamics and Materials Conference* (Baltimore, MD), AIAA, Washington, DC, April 1991, pp. 1964–1970.

[26]Ashley, H., and Zartarian, G., "Piston Theory—A New Aerodynamic Tool for the Aeroelastician," *Journal of the Aeronautical Sciences,* Vol. 23, Dec. 1956, pp. 1109-1118.

[27]Jones, R. M., *Mechanics of Composite Materials,* Scripta Book Co., Washington, DC, 1975, p. 70.

[28]Shiau, L., and Chang, J., "Flutter Analysis of Composite Panels on Many Supports," *Proceedings of the 4th International Conference in Structural Dynamics: Recent Advances,* edited by M. Petyt, H. F. Wolfe, and C. Mei, Elsevier, London, July 1991, pp. 377–386.